HHS Public Access

Author manuscript

*Mol Pharm*. Author manuscript; available in PMC 2016 July 06.

Published in final edited form as:

*Mol Pharm*. 2015 July 6; 12(7): 2528–2536. doi:10.1021/acs.molpharmaceut.5b00032.

# Chemical Analysis of Drug Biocrystals: A Role for Counterion Transport Pathways in Intracellular Drug Disposition

**Rahul K. Keswani**[§], **Jason Baik**[§,#], **Larisa Yeomans**[‡], **Chuck Hitzman**[†], **Allison Johnson**[§], **Ashtamurthy Pawate**[||], **Paul J. A. Kenis**[||], **Nair Rodriguez-Hornedo**[§], **Kathleen A. Stringer**[¶], and **Gus R. Rosania**[§,*]

[§]Department of Pharmaceutical Sciences, College of Pharmacy, 428 Church Street, University of Michigan, Ann Arbor 48109

[‡]Department of Medicinal Chemistry & Biochemical Nuclear Magnetic Resonance Core, College of Pharmacy, 428 Church Street, University of Michigan, Ann Arbor 48109

[†]Stanford Nano Center, McCullough Building, Stanford University, 476 Lomita Mall, Stanford, CA 94305

[||]Department of Chemical & Biomolecular Engineering, University of Illinois, 600 South Mathews Avenue, Urbana-Champaign, IL 61802

[¶]Department of Clinical, Social and Administrative Sciences, College of Pharmacy, 428 Church Street, University of Michigan, Ann Arbor 48109

## Abstract

In mammals, highly lipophilic small molecule chemical agents can accumulate as inclusions within resident tissue macrophages. In this context, we characterized the biodistribution, chemical composition and structure of crystal-like drug inclusions (CLDIs) formed by clofazimine (CFZ), a weakly basic lipophilic drug. With prolonged oral dosing, CFZ exhibited a significant partitioning with respect to serum and fat due to massive bioaccumulation and crystallization in the liver and spleen. The NMR, Raman and Powder X-ray diffraction (p-XRD) spectra of CLDIs isolated from the spleens of CFZ-treated mice matched the spectra of pure, CFZ hydrochloride crystals (CFZ-HCl). Elemental analysis revealed a 237-fold increase in chlorine content in CLDIs compared to untreated tissue samples, and a five-fold increase in chlorine content compared to CFZ-HCl, suggesting that the formation of CLDIs occurs through a chloride mediated crystallization mechanism. Single crystal analysis revealed that CFZ-HCl crystals had a densely-packed orthorhombic lattice configuration. *In vitro*, CFZ-HCl formed at a pH of 4–5 only if chloride ions

Corresponding Author: Gus R Rosania, Department of Pharmaceutical Sciences, University of Michigan College of Pharmacy, 428 Church St, Ann Arbor, MI 48109, USA, Phone: 734-763-1032, grosania@umich.edu.

[#]**Present Addresses:** - Now at Optivia Biotechnology Inc., 115 Constitution Dr. Suite 7, Menlo Park, CA 94025

**Author Contributions**

RKK, JB, GRR planned the study; RKK, JB, GRR, CH, LY, AJ performed the experiments; AP, PJAK provided single crystal data analysis; RKK, NRH, KAS, GRR analyzed the data and wrote the manuscript.

SUPPORTING INFORMATION AVAILABLE

Supplementary Methods, Optical Microscopy, TEM and FFEM data, NMR peak identification of clofazimine, p-XRD peaks and indexing of clofazimine crystals, single crystal structural data, Raman microscopy data, nanoSIMS plots and mass images, pH and solubility data and images of CFZ salts. This information is available free of charge via the Internet at http://pubs.acs.org/.

were present at sufficiently high concentrations (>50:1 $Cl^-$:CFZ), indicating that intracellular chloride transport mechanisms play a key role in the formation of CLDIs. While microscopy and pharmacokinetic analyses clearly revealed crystallization and intracellular accumulation of the drug *in vivo*, the chemical and structural characterization of CLDIs implicates a concentrative, chloride transport mechanism, paralleling and thermodynamically stabilizing, the massive bioaccumulation of a weakly basic drug.

**Keywords**

Clofazimine; bioaccumulation; chloride channels; intracellular crystals; pharmacokinetics

## INTRODUCTION

The elucidation of molecular mechanisms influencing the solubility of poorly soluble chemical agents in different cells, tissues and organs of mammals is interesting from a fundamental chemical and biological perspective. Cells are able to eliminate soluble chemical agents via metabolism and facilitated or active transport across the plasma membrane. Moreover, in the case of foreign, insoluble particles, phagocytic cells of the immune system are especially equipped to actively ingest these particles and isolate them from the rest of the organism. However, for poorly soluble compounds, that can exist both as soluble and insoluble forms within the cells of an organism, the mechanisms controlling the bioaccumulation and distribution of soluble and insoluble forms of these agents in the different cells and organs of the body are not known.

Many FDA-approved drugs (e.g., clofazimine, amiodarone, azithromycin, chloroquine, gefitinib) fall within the class of poorly soluble compounds that are actively sequestered within macrophages[1–6]. Elucidating the mechanisms affecting their solubility and accumulation inside cells is relevant to understanding drug toxicity, disposition and efficacy[7]. Particularly, weakly basic molecules have been implicated to be accumulated via the lysosomal pathway in macrophages due to the decrease in pH of the vesicles that contain the drug[1]. Remarkably, research into mechanisms responsible for *in vivo* drug bioaccumulation and retention has been very sparse.

While searching for drugs exhibiting natural, intracellular drug bioaccumulation mechanisms, clofazimine (CFZ) caught our attention[8–12]. CFZ is an FDA-approved riminophenazine antibiotic (Figure 1) that has been remarkably effective against mycobacterial infections such as leprosy[13–15] and mycobacterium avium infections in AIDS patients[16,17]. It has also attracted attention because of its anti-inflammatory[18,19] and immunomodulatory[20] properties, and it is especially used for treating leprotic skin inflammations (erythema leprosum nodosum)[18,19,21,22]. Here, we report on the significance of counterion transport pathways in the bioaccumulation and tissue distribution of CFZ in mammalian organisms. In particular, our studies point to a key role played by concentrative, chloride transport mechanisms in the formation or stabilization of insoluble intracellular drug complexes formed by CFZ in macrophages, upon prolonged oral administration.

## EXPERIMENTAL SECTION

### Animal experiments

Mice (4 week old, male C57Bl6) were purchased from the Jackson Laboratory (Bar Harbor, ME) and acclimatized for 1 week in a specific-pathogen-free animal facility. Animal care was provided by the University of Michigan's Unit for Laboratory Animal Medicine (ULAM), and the experimental protocol was approved by the Committee on Use and Care of Animals. Clofazimine (CFZ) (C8895; Sigma-Aldrich, St. Louis, MO) was dissolved in sesame oil (Roland, China, or Shirakiku, Japan) to achieve a concentration of 3 mg/ml, which was mixed with Powdered Lab Diet 5001 (PMI International, Inc., St. Louis, MO) to produce a 0.03% drug to powdered feed[23]. A corresponding amount of sesame oil was mixed with chow for vehicle treatment. On average, food consumption for a 25 g mouse was 3 g/day, resulting in 10 mg of bioavailable drug/kg per day. For CFZ treatment, the drug diet was carried out for 8 weeks followed by a switch to a control diet for 8 weeks (washout phase).

### Measurement of CFZ in tissues

CFZ mass was measured as previously reported[24,25]. Briefly, at predetermined time points, mice were euthanized using $CO_2$, and blood was removed through cardiac puncture. Organs and tissues were harvested, washed in cold DPBS, and kept at −20°C until further analysis. The tissues were homogenized with Tissumizer (Tekmar®, Cincinnati, OH) and CFZ was extracted with dichloromethane twice followed by solvent evaporation and resolubilization in methanol (MeOH). CFZ mass was spectrophotometrically determined in methanol (λ=490 nm) and the concentration was calculated using a standard curve generated by spiking extracted tissue of the control (vehicle-only treated) mice tissue with known amounts of drug. The tissue-to-fat partition ratios were computed based on mass of drug in the various tissues relative to mass of drug in total body fat (units: dimensionless; calculated as [mg CFZ/g tissue]/[mg CFZ/g fat]). The tissue to plasma partition ratios were computed based on mass of drug in the various tissues relative to mass of drug in plasma volume (units: $g^{-1}$ tissue, calculated as [mg CFZ/g tissue]/[mg CFZ in blood]). CFZ mass was measured in relation to the measured weight of the tissue or plasma volume.

### Isolation of CLDIs from mouse spleens

Spleen tissue homogenate at 8 weeks post drug feeding was sonicated for 30 minutes and clarified by centrifugation (100 × *g* for 1 min). Supernatant was resuspended in 10% sucrose solution in $H_2O$ followed by centrifugation (100 × *g*) to remove large cell debris. The drug inclusions in the supernatant were then pelleted by centrifugation (21,000 × *g* for 1 min) and resuspended in 20 ml of 10% sucrose. Clofazimine content was spectrophotometrically (λ=490 nm) determined using calibrated CFZ standards[23,24,26].

### Preparation and transmitted light microscopy of cryopreserved tissues

After euthanasia, organs removed from CFZ and vehicle fed mice were cryo-preserved in optimal cutting temperature compound (Tissue-Tek 4583; Sakura). Tissue blocks were sectioned at a thickness 10 μm, using a Leica 3050S cryostat. For transmitted microscopy,

cryo-sectioned slices were mounted on glass slides with glycerol, and imaged with Olympus X51 upright microscope equipped with X100 objective, DP-70 color camera, and DP controller 3.1.1267.

### Sample Preparation and Transmission Electron Microscopy (TEM)

For TEM, mice were euthanized and they were perfused blood-free by infusing 0.1 M Sorensen's buffer into left ventricle. After flushing for five minutes, five times the total blood volume of fixative containing Karnovsky's solution (3% paraformaldehyde, 2.5% glutaraldehyde) was infused. Afterwards, organs were removed, minced, and kept in the fixative solution at 4 °C until further processing. For staining, the tissues were incubated with osmium tetroxide and dehydrated in alcohol. Dehydrated samples were infiltrated with Epon resin and then polymerized at 60 °C for 24 hours. The polymerized tissue blocks were sectioned with an ultramicrotome and post-stained with uranyl acetate and lead citrate. TEM was performed with a Philips CM-100 instrument equipped with a Hamamatsu ORCA-HR camera system operated by Advanced Microscopy Techniques (Danvers, MA).

### Synthesis of CFZ crystals

CFZ was dissolved in MeOH at 2 mM. Equal volumes of anti-solvents were added to obtain the drug crystals − 0.1 M HCl – CFZ-A1, 0.1 M NaOH – CFZ-B, $H_2O$ – CFZ-N, 1 M $NH_4Cl$ – CFZ-A2. The supernatant was removed, and the crystals were washed and lyophilized in the dark in preparation for further analysis.

### Powder X-ray diffraction (p-XRD)

Powder XRD of dried samples of isolated CLDIs, 8 week treated (or vehicle) mouse tissue homogenate and synthetic CFZ samples were carried out with Bruker D8 Advance - Cu $K_\alpha$ radiation ($\lambda$ = 1.5406 Å), tube voltage = 40 kV, tube current = 40 mA. Data were collected at $2\theta$=4° to 40° at a continuous scan at the rate of 2.5°/min. Diffractograms of the triclinic (DAKXUI01) and monoclinic (DAKXUI) forms of CFZ crystals were imported from Cambridge Structural Database (CSD) and CFZ-TC crystals (C8895; Sigma-Aldrich, St. Louis, MO) were used as a positive control for comparison.

### Solution NMR

1D $^1$H-NMR and 2D HSQC spectra for various CFZ samples and CLDIs were acquired at the University of Michigan's Biochemical NMR Core Laboratory using an 11.74 Tesla (500 MHz) NMR spectrometer with a VNMRS console and a 7510-AS autosampler system operated by host software VNMRJ 3.2, and equipped with a 5 mm Agilent OneNMR probe with Z-axis gradients. DMSO-d6 (100%, 99.9% atom % D) was purchased from Cambridge Isotope Laboratories, Inc. (Tewksbury, MA). The samples were prepared by first freeze-drying the samples overnight followed by dissolution in DMSO-d6 at 2 mg/ml. 128 ($^1$H) and 8 (HSQC) scans were acquired for each sample. For accurate identification of the NMR peaks in spectrum, a DMSO-d6-solubilized CFZ spectrum was acquired from a saturated solution of CFZ in DMSO: $^1$H 64 scans; $^{13}$C 9000 scans; HMBC 32 scans; HSQC (gc2hsqcse was the pulse sequence) 8 scans; COSY (DQF-COSY) 8 scans; NOESY 8 scans. All the experiments were run at 25 °C and using the standard parameters from VNMRJ4.0

(Agilent Technologies). All the data were processed with MestreNova 9.0 (MestreLab, Santiago de Compostela, Spain).

### Bulk Elemental Composition Analysis (BEA)

CFZ samples were pelleted via centrifugation (10,000 × *g*, 2 min) followed by removal of supernatant and freeze-drying overnight. All samples were sent to Atlantic Microlab, Inc. (Norcross, GA) for elemental analysis. Established protocols for the measurement of carbon (C), hydrogen (H), nitrogen (N), chlorine (Cl) and sulfur (S) were used to obtain elemental data. All instrumentation used were calibrated daily with ultra-high purity standards. In brief, samples were accurately weighed using electronic microbalances. C, H, N and S analyses were performed on automatic analyzers based on a modified Pregl and Dumas methodology wherein samples were flash combusted in an oxygen atmosphere at ~1400 °C. Quantitative combustion was achieved by passing the mixture of gases over oxidizing agents comprised of copper oxide, EA1000 (chromium and nickel oxide mixture) and tungstic anhydride, and then over copper, maintained at 650 °C, to remove excess oxygen and to reduce the oxides of N. The individual components were separated and eluted as $CO_2$, $H_2O$, $N_2$ and $SO_2$ followed by measurement via a thermal conductivity detector. Cl analysis was performed by Schoniger flask combustion followed by analysis using ion chromatography. The sample was diluted to 25 ml, 50 ml, or 75 ml, filtered and injected into the IC to yield the ppm levels of Cl. All samples were analyzed in duplicate by different technicians.

### Secondary Ion Mass Spectroscopy (nanoSIMS)

CFZ-TC and other crystals of CFZ were prepared as mentioned earlier and deposited onto Si wafers and allowed to dry overnight. For CLDI samples, spleens from 8 week CFZ fed mice were isolated and cryo-preserved in optimal cutting temperature compound (Tissue-Tek 4583; Sakura) for histological sectioning as mentioned above. The sections were then scrapped off gently onto a Si wafer. The spatial distribution of various atomic species along the depth of the sample in cross-sectional pattern was mapped with the Cameca NanoSIMS ion micro-probe (CAMECA Instruments, Inc., Madison, WI, USA). Briefly, with a primary beam of Cs+, focused to a spot-size of 200 nm on the gold-coated surface of the sample, secondary ions of $^{12}C$, $^{16}O$, $^{14}N$, $^{28}Si$, $^{32}S$, $^{31}P$, $^{35}Cl$ were sputtered from the sample surface and detected simultaneously in multi-collector mode. Elemental composition was obtained by comparing counts with respect to CFZ-TC as a calibration standard for all atomic species.

### X-Ray Crystallography

Diffraction patterns of CFZ crystals were obtained on a Rigaku Saturn 944+ (Cu $K_\alpha$ ($\lambda$=1.54178 Å)) at −188 °C. Data reduction was performed using CrysAlisPro (Agilent Technologies), and the structure was solved with direct methods using SHELXS[27]. Structure building, refinement, and electron density map generation were done with SHELXL via the ShelXle GUI[28]. Mercury was used to visualize the crystal structure, access CCDC database as well as obtain predicted p-XRD data.

### Data Plotting and Statistical Analysis

All statistical analysis was performed using either ANOVA or Student's t-test. Results were considered significant if $p \leq 0.05$. Plots were constructed using Origin 9.0 (OriginLab Corporation, Northampton, MA, USA) and laid out in figure format using scalable vector graphics format (svg) in either Inkscape (www.inkscape.org) or GIMP (www.gimp.org). NMR plots were constructed in MestreNova 9.0 (MestreLab, Santiago de Compostela, Spain).

## RESULTS

Clofazimine (CFZ) – $C_{27}H_{22}Cl_2N_4$ - is a weakly basic, small molecule chemical agent with a calculated $pK_{a1} = 2.31$ and $pK_{a2} = 9.29$ and is highly lipophilic (clog P ~ 7). Like other lipophilic weak bases, it has a long retention time within tissues, and exhibits a highly variable pharmacokinetic half-life ($t_{1/2}$~70 days in humans, 7 days in mice)[9]. Upon oral dosing, CFZ exhibits context-dependent pharmacokinetics; while its half-life is in the order of hours to days after an acute dose, upon prolonged oral administration, its half-life is in the order of weeks to months[9,29,30]. In aqueous solution, CFZ predictably exists in neutral, monoprotonated and diprotonated states depending on the solution pH (Figure 1)[31]. Commercially, CFZ is available as a triclinic polymorph of the unprotonated drug (CFZ-TC; Sigma:C8895).

To study the intracellular disposition of CFZ upon prolonged oral dosing, CFZ-TC was fed to 4–5 week old C57Bl/6 mice for at least 8 weeks as an oral diet mixed with sesame oil and regular chow (150 mg, 100 ml, 500 g respectively). Following 3–8 weeks of oral administration, CFZ progressively accumulated within macrophages as membrane-bound crystal-like drug inclusions (CLDIs)[23,24] in the spleen and liver (Figure 2, **S2–S3**). As expected based on the tendency of hydrophobic small molecules to partition into body fat, CFZ concentration in adipose tissue was >10,000-fold greater than in serum, starting at three weeks (Figure 2a). However, by eight weeks of treatment, tissue-to-serum partition ratios in spleen, liver and intestine dramatically increased and surpassed fat-to-serum partition ratios, relative to three weeks and then remained relatively constant during an eight week washout period (Figure 2a), suggesting a special sequestration mechanism determining the preferential accumulation and retention of CFZ in these organs relative to body fat. Analyzing the distribution of CFZ revealed that spleen, liver and intestine were major sites of drug retention, after the eight week washout period (Figure 2a). Based on measured partition ratios as well as the mass of drug remaining after the washout period, CFZ mass retained in spleen exceeded its combined mass retained in the other organs (Figure 2a).

To study the sites of CFZ retention, we used transmitted light microscopy and transmission electron microscopy (TEM) to visualize tissue cryo-sections of spleen and liver (Figure 2b). CLDIs were observed in the eight week treated mice and even after drug treatment was discontinued (washout phase) in the spleen, liver and intestines (Figures S2–S3). The intracellular localization and morphology of CLDIs was also independently established using TEM. The spleens of CFZ-treated mice and those of washout animals exhibited cells filled with empty, elongated, and polyhedral CLDI cavities that remained after the drug was extracted during TEM sample preparation process (Figure 2b). In TEM images, CLDI

cavities exhibited faceted, polygonal shapes, with multiple CLDIs clustered within organelle-free cytoplasmic subdomains. In the liver, Kupffer cells were filled with CLDI cavities and arranged in clusters, as previously reported[23,24]. Most importantly, after an eight week washout period, intracellular CLDI cavities were still present within clusters of Kupffer cells (Figure 2b). Overall, other organelles, including endolysosomal vesicles, mitochondria, nuclei, Golgi were generally localized at the periphery of CLDI clusters[24]. Nuclear morphology of the cells containing CLDIs was normal and similar to that of CLDI-free cells, without any evidence of nuclear condensation or fragmentation which would suggest necrosis or apoptosis.

Deep-Etch Freeze-Fracture Electron Microscopy (FFEM) was used to inspect the interface between the internal core of the CLDI and the cytoplasm at high magnification (Figure S4). We observed that each CLDI was surrounded by a ~40 nm thick, multilamellar structure comprised of five distinct layers, with morphological features that were unlike those of any membranes surrounding the other cellular organelles. In direct frontal views of cross-sectional profiles of CLDIs, the membrane layers lacked regular lattice spacings and cleavage planes that characterized the underlying structure of the CLDI cores. Examining this cell-crystal interface revealed a complex arrangement of five distinct membranous layers (Figure S4, 1 to 5). Also observed surrounding the CLDIs were other organelles including mitochondria, lysosomes, endoplasmic reticulum and nuclei. However, none of the membranes delimiting these other organelles exhibited the characteristic morphological features of the multi-lamellar structure that was consistently observed at the CLDI-cell interface.

Thus, CLDIs reflect an increase in the partition coefficient of CFZ into these tissues, relative to body fat (Figure 2, Figures S2–S4). Considering the massive crystallization of the drug, we focused our efforts toward thorough chemical analysis of drug precipitates obtained both biologically as well as through *in vitro* chemical synthesis. To obtain synthetic drug precipitates, CFZ was recrystallized through the addition of acidic or basic solvents to pure drug solutions in methanol. The addition of basic (0.1 M NaOH) or neutral ($H_2O$) anti-solvent led to the formation of orange-colored precipitates (Figure 1), CFZ-B and CFZ-N, respectively. In contrast, the addition of acidic (0.1 M HCl, pH 0.9–1) or 1 M $NH_4Cl$ (pH 4–5) solutions resulted in dark-red precipitates (Figure 1), CFZ-A1 and CFZ-A2 that looked similar to CLDIs. On the other hand, the orange color of CFZ-B and CFZ-N was similar to that of CFZ-TC. To obtain intracellularly crystallized samples, CLDIs were isolated from the eight week CFZ-treated animal spleen via organ rupture followed by centrifugation.

The protonation state of the CFZ molecule in the different CFZ crystals and CLDIs was examined via solution NMR studies, conducted in DMSO-d6. $^1$H NMR of CFZ-A1 and CFZ-A2 revealed a chemical shift of $+\delta_a$=0.25 ppm and $+\delta_b$=0.15 ppm for the aliphatic protons (1–7, Figure 1) compared to CFZ-TC, noticeably brought about by the protonation of the amine - 22 ($pK_{a2}$, Figure 1, Figure 3a). The $^{13}$C, HSQC, HMBC, COSY, NOESY spectra comparing $^1$H with their carbons (Figures S5–S15) and $^1$H integration (Table S1) was used to assign NMR peaks to the protons in the molecule. All other protons also exhibited varying chemical shifts ($+\delta$=0.05–0.6 ppm) in CFZ-A1 and CFZ-A2 relative to CFZ-TC. Most importantly, CLDIs isolated from the spleen, CFZ-A1 and CFZ-A2 showed

similar $^{1}$H NMR spectra with an additional amine proton (22) that was absent in CFZ-TC (Figure 3a). Thus, the NMR spectra indicate that CFZ present in CFZ-A1 and CFZ-A2 crystals and, most importantly, in CLDIs is monoprotonated.

Bulk elemental analysis (BEA) was then performed to determine the exact elemental composition of CFZ-A1, CFZ-A2 and CFZ-TC. Using the ratio N/Cl as a direct indicator of the stoichiometry of Cl in relation to the number of protonatable amines, BEA confirmed the presence of an additional Cl in CFZ-A1 and CFZ-A2 relative to CFZ-TC (CFZ-A1 and CFZ-A2 had an N/Cl = 1.33 whereas in CFZ-TC, N/Cl = 2; Table 1). This confirmed that CFZ-A1 and CFZ-A2 were identical in chemical composition, confirmed to be the monoprotonated hydrochloride salt of CFZ, hereby referenced as CFZ-HCl. Since, CLDIs were derived from a biological source and contained cellular-derived impurities in the form of membranous domains (Figures S2–S4), bulk elemental analysis to determine sample stoichiometry would provide an erroneous chemical composition. Hence, CLDIs were analyzed with Secondary Ion Mass Spectroscopy (nanoSIMS) to obtain localized mass distributions within crystals along with other synthetic CFZ crystals. With this instrument, the measured, integrated ion counts are proportional to the elemental composition of the sputtered surface. The counts were plotted in relation to the position of the atom beam to generate a mass image of each isotope in a sample. By progressively scanning a region of a sample, depth profiles of atom counts through the samples were obtained (Figures S16–S17). To compare atomic composition of CLDIs and reference CFZ crystals, C, N, S, O, P, and Si isotope counts were divided by the corresponding Cl counts and adjusted for differences in detector yield using CFZ-TC as a calibration standard (Table 2). Accordingly, the N/Cl ratio for CFZ-HCl was identical to the value obtained via BEA (=1.33) and lower than CFZ-TC (=2) (Table 1), consistent with the theoretical stoichiometry of Cl per the chemical formula of CFZ-HCl. More remarkably, N/Cl for Spleen CLDIs was 237-fold lower compared to the tissue only sample (no drug) (Table 2, Figures S16–S17). This is consistent with a high concentration of chloride within CLDIs relative to the rest of the cell. While there was a high concentration of P, S, Si and O in the surrounding tissue and in untreated tissue samples (P/Cl = 0.128, S/Cl = 0.917, Si/Cl = 0.123, O/Cl = 1.704), P, S and Si were undetectable in CLDIs. O was marginally present with O/Cl = .022. The C/Cl ratio demonstrated a much higher accumulation of carbon within CLDIs (23.16) in relation to expected carbon counts based on pure CFZ crystals –CFZ-TC (13.5) and CFZ-A1/A2 (4.43) but much lower than only tissue (81.59). The detection of minor oxygen content and excess carbon in CLDIs confirms the presence of non-drug derived impurities in the form of biological membranes.

To probe the crystal structures of CLDIs in relation to its different crystal forms, powder X-Ray Diffraction (p-XRD) was performed on samples of isolated spleen CLDIs, CFZ-TC, CFZ-A1 and CFZ-A2. The diffraction peak corresponding to $2\theta = 9.3°$ (d=9.71 Å) was present exclusively to CFZ-TC (Figure 3b, closest crystal analog CCDC refcode – DAKXUI01, Figure S18, Table S2)[32], while the plane corresponding to $2\theta = 7.3°$ (d=12.27 Å) was exclusive to CLDIs, CFZ-A1 and CFZ-A2 (Figure 3b, Table S2). This single peak was previously reported as being a hallmark of spleen CLDIs[24]. Hence this particular peak can be considered a signature peak for CFZ-HCl crystals. Additional peaks that were observed in CFZ-A2 ($2\theta = 22.8°, 32.7°$) relative to CFZ-A1 were attributable to unreacted,

contaminating $NH_4Cl$ crystals. Other prominent peaks were uniquely present in CLDIs, CFZ-A1 and CFZ-A2 (peaks shown in red, Figure 3b, Table S2). Also, observed were peaks common to CFZ-TC, CFZ-A1, CFZ-A2 and CLDIs (peaks shown in blue, Figure 3b, Table S2; peaks exclusive to CFZ-TC are shown in green). Thus, the p-XRD data clearly indicates that CFZ in CLDIs is present in a structural organization similar to that of pure CFZ-HCl crystals (both CFZ-A1 and CFZ-A2). To further confirm the similarity of the crystallized microstructure of CLDIs relative to CFZ-HCl, Raman microspectroscopy was performed. Peaks observed in CFZ-TC are shown in green while those observed in CFZ-HCl are shown in red (Figure S19). Consistent with the p-XRD observations, the Raman spectra of CLDIs and CFZ-HCl were similar, exhibiting matching peaks at 1396 $cm^{-1}$ and 1301 $cm^{-1}$. These peaks were absent in the Raman spectra of CFZ-TC.

While the X-ray diffraction signals acquired from single CLDIs were not useful in terms of constructing a 3D molecular model, noting the fact that CLDIs and CFZ-HCl are structurally and chemically similar (Figure 3b), CFZ-HCl crystals were subjected to single crystal analysis. The structure revealed an orthorhombic configuration with 8 molecules/unit cell in CFZ-HCl (submitted to CCDC – Cambridge Crystallographic Data Center, deposition number: 1053818) compared to CFZ-TC (CCDC refcode: DAKXUI01, triclinic, 2 molecules/unit cell) (Figure 4, Table S3). The stacking of CFZ in CFZ-HCl was remarkably closer than in CFZ-TC with the phenazine backbones being 5.32 Å apart within a dual molecule stack while that in CFZ-TC being 12.15 Å. The phenazine backbone had an inherent torsion of 9.4° in CFZ-HCl and 1.58° in CFZ-TC. The densely packed CFZ-HCl had a calculated density of 1.36 g/ml while CFZ-TC had a density of 1.3 g/ml. The signature peak of CLDIs at $2\theta = 7.3°$ (Figure 3b) was indexed as the 002 plane in the crystal lattice (Table S4) while the signature peak of CFZ-TC at $2\theta = 9.3°$ (Figure 3b) was indexed as the 001 plane in the lattice (Table S5). Significantly, the predicted p-XRD pattern of the CFZ-HCl based upon its orthorhombic configuration also matched with the absolute p-XRD pattern (Figure S20, Table S2). Overall, since the p-XRD pattern of CLDIs match those of CFZ-HCl (Figure 3b), it can be inferred that CLDIs predominantly contain layers of CFZ as orthorhombic crystalline structures of CFZ-HCl (Table S3) separated by membranes of likely biological origin, consistent with the three dimensional, orthogonal orientation of cleavage faces and fracture plane observed by deep etch-freeze fracture electron microscopy (Figure S4). Further refinement of the crystal structure is ongoing.

## DISCUSSION

CFZ was recently found to be effective against multidrug resistant tuberculosis and is currently in clinical trials for this indication[18,33–36]. This has prompted increased interest in understanding the mechanism underlying its atypical pharmacokinetic properties since the drug's bioaccumulation and pharmacokinetics has been shown to be dependent on the treatment period and dosing. Our results provide evidence that a solution-to-solid phase transition, more specifically the formation and stabilization of an intracellular, crystalline hydrochloride salt form of the drug, is responsible for the high tissue-to-serum partition coefficients of CFZ in spleen and liver. Such massive sequestration of CFZ as crystal-like drug inclusions (CLDIs) in the macrophages of spleen[10], liver[22] and intestines[37] as well as lung[8] has been reported in humans. In previous studies, we and others have shown that

CLDIs originate from a multi-lamellar, membrane-bound perinuclear cytoplasmic structure, with morphological characteristics resembling autophagosomes derived from degenerating lysosomes, mitochondria and perhaps other organelles[8,12,24,26,31,38,39]. In this study, we further demonstrate via transmission and deep-etch freeze fracture electron microscopy that the membranes bounding the CLDIs are indeed very different from the membranes bounding the typical cytoplasmic organelles: a well-structured, multilamellar membrane possessing five distinct, different layers can be clearly seen in many different CLDIs (Figure S4). However, the molecular transport mechanisms leading to cell and tissue specific, drug biocrystal formation and stabilization have not been explored.

Following quantitative, chemical and structural analyses on CLDIs isolated from mice spleens, our results provide mechanistic insights for the bioaccumulated crystallization. While many biological anions (e.g., chloride, phosphate, sulfate, carbonate, oxalate) could form salt crystals with the ionized, protonated CFZ, chemical characterization of CLDIs using powder X-Ray Diffraction (Figure 3b), $^{1}$H NMR (Figure 3a), Raman Microspectroscopy (Figure S19) and nanoSIMS (Table 2) suggest that chloride is essential for the crystallization of CFZ in CLDIs. The nanoSIMS data clearly shows that the high levels of chloride observed in CLDIs far exceed chloride levels observed in untreated tissue samples or in the other cell-derived material that is around the CLDIs. Thus, different lines of evidence point to the importance of concentrative chloride transport pathways in the context of the mechanism of CLDI formation and stabilization. Furthermore, the relative absence of oxygen, phosphorus and sulfur in CLDIs relative to the surrounding tissue suggests that this concentrative mechanism is specific to chloride, and not to other common anions present inside cells. The higher than expected O/Cl and C/Cl values could reflect the presence of biologically-derived membrane domains separating layers of pure CFZ-HCl in CLDIs, as suggested by deep-etch freeze fracture electron microscopy analysis of CLDIs (Figure S4)[24].

With regards to the specific accumulation of CLDIs in macrophages, it is expected that the endolysosomal network within the cells would play a critical role in such chloride-mediated precipitation events. The macrophage endo/phago/lysosomal network has a pH range of 4–6[40,41] and also possess $Cl^{-}/H^{+}$ channels, such as the ClC-7 anti-porter, which can provide not only a primary chloride permeation pathway within lysosomes[42], but also a potential concentrative, chloride transport mechanism. Other chloride channels that are present in macrophage lysosomes include the CFTR and ClC-1, both of which have been implicated as modulators of phagosomal maturation[43]. As a weakly basic, lipophilic molecule, CFZ is expected to accumulate in acidic organelles like endosomes and lysosomes. Nevertheless, CFZ has also been shown to interact with the membranes of mitochondria and perhaps other organelles[26]. This is not too surprising, because CFZ is a highly lipophilic molecule and is therefore prone to partition nonspecifically into hydrophobic core of cellular membranes. Since the flux of chloride ions across cellular membranes is highly regulated by specific ion channels, the results of the present study implicate these chloride channels in stabilizing CFZ in CLDIs (as the CFZ-HCl salt). Because the multilamellar membrane structure that we have found to surround the CLDIs (Figure S4) is an atypical characteristic of lysosomes, endosomes or phagosomes, the precise identity of the organelle that may be mediating and stabilizing CLDI formation remains to be determined.

To study how high, local chloride concentrations may thermodynamically stabilize and perhaps drive intracellular CLDI formation, we studied the formation of CFZ precipitates under *in vitro* conditions. Precipitation of CFZ by diluted HCl alone (0.1–0.01 mM, pH=5–6) resulted in the formation of precipitates that resembled CFZ-N or CFZ-B (Figure S21), while the precipitation of CFZ by $NH_4Cl$ at high concentrations (0.1–1 M) yielded deep red monoprotonated CFZ-HCl crystalline precipitates at pH ~5 (Figure S22, Table S6). However, as $NH_4Cl$ was diluted to concentrations < 100 mM (<50:1 $Cl^-$:CFZ), CFZ again precipitated as yellow-orange aggregates of unprotonated, neutral CFZ (Table S6). Furthermore, CFZ was completely solubilized in aqueous media, only at very acidic pH, under conditions in which clofazimine is most likely found in a diprotonated state (<1, ~5 M HCl) (Figure S22)[31]. However, formation of monoprotonated CFZ at pH ~5 in the presence of >0.1 M $NH_4Cl$, was stabilized as a precipitated salt in the form of CFZ-HCl crystals, rather than remain in solution (Figure S23). Based on these observations, we postulate that crystallization and stabilization of CFZ-HCl as CLDIs at the physiological pH of acidic organelles (also pH~5) must be dependent on molecular mechanisms that facilitate proton and excess chloride transport.

To further establish the specific molecular pathway facilitating chloride transport into CLDIs, experiments using pharmacological inhibitors of transmembrane chloride channels, as well as specific mice mutants with defects in transmembrane chloride transport mechanisms are in progress. In terms of potential implications of these observations to other drugs, in addition to CFZ, weakly basic drugs have been reported to accumulate in lysosomes while undergoing solution-to-solid phase transitions[7]. Nevertheless, beyond pH-dependent ion trapping mechanisms, the detailed chemical and structural analysis presented in this study indicate that, specific counterion transport pathways also need to be considered in order to fully understand the intracellular transport and disposition properties of weakly basic drugs.

## Supplementary Material

Refer to Web version on PubMed Central for supplementary material.

## Acknowledgments

This work was supported by the National Institute of General Medical Sciences (NIGMS; R01GM078200 to GRR) and the University of Michigan's M-Cubed initiative (http://mcubed.umich.edu). The content is solely the responsibility of the authors and does not necessarily represent the official views of the NIGMS or the National Institutes of Health. GRR is a consultant for Bristol-Myers Squibb. There are no other competing financial interests. We thank Sudha Sud (College of Pharmacy, University of Michigan) for help with in vivo experiments and sample procurement, W.G. Rajeswaran (Vahlteich Medicinal Chemistry Core, University of Michigan) and Julie Trexel (College of Pharmacy, University of Michigan) for their help in NMR sample prep and analysis, Antek Wong-Foy (Department of Chemistry Technical Services, University of Michigan) for help on p-XRD, Jeff Kampf (Department of Chemistry Technical Services, University of Michigan) for acquiring single crystal structure data, Robyn Roth & Dotty Sorenson (Microscopy & Image Analysis Core, University of Michigan) for help with freeze-fracture EM and TEM.

## References

1. Ohkuma S, Poole B. Cytoplasmic Vacuolation of Mouse Peritoneal Macrophages and the Uptake into Lysosomes of Weakly Basic Substances. J Cell Biol. 1981; 90:656–664. [PubMed: 7287819]

2. Poole B, Ohkuma S. Effect of Weak Bases on the Intralysosomal pH in Mouse Peritoneal Macrophages. J Cell Biol. 1981; 90:665–669. [PubMed: 6169733]
3. Maxfield FR. Weak Bases and Ionophores Rapidly and Reversibly Raise the pH of Endocytic Vesicles in Cultured Mouse Fibroblasts. J Cell Biol. 1982; 95:676–681. [PubMed: 6183281]
4. Quaglino D, Ha HR, Duner E, Bruttomesso D, Bigler L, Follath F, Realdi G, Pettenazzo A, Baritussio A. Effects of Metabolites and Analogs of Amiodarone on Alveolar Macrophages: Structure-Activity Relationship. Am J Physiol Lung Cell Mol Physiol. 2004; 287:438–447.
5. Bergman E, Forsell P, Persson EM, Knutson L, Dickinson P, Smith R, Swaisland H, Farmer MR, Cantarini MV, Lennernäs H. Pharmacokinetics of Gefitinib in Humans: The Influence of Gastrointestinal Factors. Int J Pharm. 2007; 341:134–142. [PubMed: 17482782]
6. Gladue RP, Bright GM, Isaacson RE, Newborg MF. In Vitro and In Vivo Uptake of Azithromycin (CP-62, 993) by Phagocytic Cells: Possible Mechanism of Delivery and Release at Sites of Infection. Antimicrob Agents Chemother. 1989; 33:277–282. [PubMed: 2543276]
7. Fu D, Zhou J, Zhu WS, Manley PW, Wang YK, Hood T, Wylie A, Xie XS. Imaging the Intracellular Distribution of Tyrosine Kinase Inhibitors in Living Cells with Quantitative Hyperspectral Stimulated Raman Scattering. Nat Chem. 2014; 6:614–622. [PubMed: 24950332]
8. Harbeck RJ, Worthen GS, Lebo TD, Peloquin CA. Clofazimine Crystals in the Cytoplasm of Pulmonary Macrophages. Ann Pharmacother. 1999; 33:250. [PubMed: 10084424]
9. Levy L. Pharmacologic Studies of Clofazimine. Am J Trop Med Hyg. 1974; 23:1097–1109. [PubMed: 4611255]
10. Aplin RT, McDougall AC. Identification of Crystals of the Rimino-Phenazine Compound B663 (Lamprene: Clofazimine) in Mouse Spleen Macrophages by Thin Layer Chromatography and Mass Spectrum Analysis. Experientia. 1975; 31:468–469. [PubMed: 1120525]
11. McDougall AC, Horsfall WR, Hede JE, Chaplin AJ. Splenic Infarction and Tissue Accumulation of Crystals Associated with the Use of Clofazimine (Lamprene; B663) in the Treatment of Pyoderma Gangrenosum. Br J Dermatol. 1980; 102:227–230. [PubMed: 7387877]
12. McDougall AC. Electron Microscope Studies of the Antileprosy Drug B663 (Clofazimine; Lamprene). Int J Lepr Other Mycobact Dis. 1974; 42:1–12. [PubMed: 4369980]
13. Tolentino JG, Rodriguez JN, Abalos RM. Controlled Long-Term Therapy of Leprosy with B663 (Lamprene, Clofazimine) Compared with DDS. Int J Lepr Other Mycobact Dis. 1974; 42:416–418. [PubMed: 4617720]
14. Karuru ER. Clinical Evaluation of Lamprene (Geigy) A Preliminary Report. Lepr Rev. 1970; 41:83–88. [PubMed: 5453083]
15. Leiker DL, Blenska W, Carling D, Fitzherbert M, Larssen P. Bacteriological Effect of Lamprene (Clofazimine) in Lepromatous Leprosy. Lepr Rev. 1971; 42:125–130. [PubMed: 4948481]
16. Van Rensburg CEJ, Joont GK, Sullivan JFO, Anderson R, Van RCE, Joone GK, O'Sullivan JF, Van Constance EJR, van Rensburg CEJ. Antimicrobial Activities of Clofazimine and B669 Are Mediated by Lysophospholipids. Antimicrob Agents Chemother. 1992; 36:2729–2735. [PubMed: 1482140]
17. Reddy VM, O'Sullivan JF, Gangadharam PRJ. Antimycobacterial Activities of Riminophenazines. J Antimicrob Chemother. 1999; 43:615–623. [PubMed: 10382882]
18. Cholo MC, Steel HC, Fourie PB, Germishuizen WA, Anderson R. Clofazimine: Current Status and Future Prospects. J Antimicrob Chemother. 2012; 67:290–298. [PubMed: 22020137]
19. Helmy HS, Pearson JMH, Waters MFR. Treatment of Moderately Severe Erythema Nodosum Leprosum with Clofazimine - A Controlled Trial. Lepr Rev. 1972; 42:162–177.
20. Ren YR, Pan F, Parvez S, Fleig A, Chong CR, Xu J, Dang Y, Zhang J, Jiang H, Penner R, et al. Clofazimine Inhibits Human Kv1.3 Potassium Channel by Perturbing Calcium Oscillation in T Lymphocytes. PLoS One. 2008; 3:e4009. [PubMed: 19104661]
21. Barry VC, Conalty ML. The Antimicrobial Activity of B663. Lepr Rev. 1965; 36:3–7. [PubMed: 14241918]
22. Barry VC, Belton JG, Conalty ML, Denneny JM, Edward DW, O'Sullivan JF, Twomey D, Winder F. A New Series of Phenazines (rimino Compounds) with High Antituberculosis Activity. Nature. 1957; 179:1013–1015. [PubMed: 13430770]

23. Baik J, Stringer KA, Mane G, Rosania GR. Multiscale Distribution and Bioaccumulation Analysis of Clofazimine Reveals a Massive Immune System-Mediated Xenobiotic Sequestration Response. Antimicrob Agents Chemother. 2013; 57:1218–1230. [PubMed: 23263006]
24. Baik J, Rosania GR. Macrophages Sequester Clofazimine in an Intracellular Liquid Crystal-like Supramolecular Organization. PLoS One. 2012; 7:e47494. [PubMed: 23071814]
25. Venkatesan K, Deo N, Gupta UD. Tissue Distribution and Deposition of Clofazimine in Mice Following Oral Administration with or without Isoniazid. Arzneim Forsch. 2007; 57:472–474. [PubMed: 17803061]
26. Baik J, Rosania GR. Molecular Imaging of Intracellular Drug-Membrane Aggregate Formation. Mol Pharm. 2012; 8:1742–1749. [PubMed: 21800872]
27. Sheldrick GM. A Short History of SHELX. Acta Crystallogr Sect A. 2008; 64:112–122. [PubMed: 18156677]
28. Hübschle CB, Sheldrick GM, Dittrich B. ShelXle: A Qt Graphical User Interface for SHELXL. J Appl Crystallogr. 2011; 44:1281–1284. [PubMed: 22477785]
29. Banerjee DK, Ellard GA, Gammon PT, Waters MFR. Some Observations on the Pharmacology of Clofazimine. Am J Trop Med Hyg. 1974; 23:1110–1115. [PubMed: 4429180]
30. Nix DE, Adam RD, Auclair B, Krueger TS, Godo PG, Peloquin CA. Pharmacokinetics and Relative Bioavailability of Clofazimine in Relation to Food, Orange Juice and Antacid. Tuberculosis. 2004; 84:365–373. [PubMed: 15525560]
31. O'Connor R, O'Sullivan JF, O'Kennedy R. The Pharmacology, Metabolism and Chemistry of Clofazimine. Drug Metab Rev. 1995; 27:591–614. [PubMed: 8925720]
32. Rychlewska U, Broom MBH, Eggleston DS, Hodgson DJ. Antileprosy Dihydrophenazines. Structural Characterization of Two Crystal Forms of Clofazimine and of Isoclofazimine, B.3857. J Am Chem Soc. 1985; 107:4768–4772.
33. Ahmad S, Mokaddas E. Current Status and Future Trends in the Diagnosis and Treatment of Drug-Susceptible and Multidrug-Resistant Tuberculosis. J Infect Public Health. 2013:1–17. [PubMed: 23290087]
34. Lu Y, Zheng M, Wang B, Fu L, Zhao W, Li P, Xu J, Zhu H, Jin H, Yin D, et al. Clofazimine Analogs with Efficacy against Experimental Tuberculosis and Reduced Potential for Accumulation. Antimicrob Agents Chemother. 2011; 55:5185–5193. [PubMed: 21844321]
35. Tyagi S, Ammerman NC, Li S-Y, Adamson J, Converse PJ, Swanson RV, Almeida DV, Grosset JH. Clofazimine Shortens the Duration of the First-Line Treatment Regimen for Experimental Chemotherapy of Tuberculosis. Proc Natl Acad Sci U S A. 2015:2–7.
36. Gopal M, Padayatchi N, Metcalfe JZ, O'Donnell MR. Systematic Review of Clofazimine for the Treatment of Drug-Resistant Tuberculosis. Int J Tuberc Lung Dis. 2013; 17:1001–1007. [PubMed: 23541151]
37. Belaube P, Devaux J, Pizzi M, Boutboul R, Privat Y. Small Bowel Deposition of Crystals Associated with the Use of Clofazimine (Lamprene) in the Treatment of Prurigo Nodularis. Int J Lepr Other Mycobact Dis. 1983; 51:328–330. [PubMed: 6685693]
38. Vandeputte D, Jacob W, Van Grieken R, Boddingius J. Study of Intracellular Deposition of the Anti-Leprosy Drug Clofazimine in Mouse Spleen Using Laser Microprobe Mass Analysis. Biol Mass Spectrom. 1993; 22:221–225. [PubMed: 8481409]
39. Conalty ML, Jina AG. The Antileprosy Agent Clofazimine (B.663) in Macrophages: Light, Electron Microscopy and Function Studies. RES Host Def. :323–331.
40. Russell DG, Vanderven B, Glennie S, Mwandumba H, Heyderman R. The Macrophage Marches on Its Phagosome: Dynamic Assays of Phagosome Function. Nat Rev Immunol. 2009; 9:594–600. [PubMed: 19590530]
41. Luzio JP, Mullock BM, Pryor PR, Lindsay MR, James DE, Piper RC. Relationship between Endosomes and Lysosomes. Biochem Soc Trans. 2001; 29:476–480. [PubMed: 11498012]
42. Graves AR, Curran PK, Smith CL, Mindell JA. The Cl−/H+ Antiporter ClC-7 Is the Primary Chloride Permeation Pathway in Lysosomes. Nature. 2008; 453:788–792. [PubMed: 18449189]
43. Jiang L, Salao K, Li H, Rybicka JM, Yates RM, Luo XW, Shi XX, Kuffner T, Tsai VWW, Husaini Y, et al. Intracellular Chloride Channel Protein CLIC1 Regulates Macrophage Function through Modulation of Phagosomal Acidification. J Cell Sci. 2012; 125:5479–5488. [PubMed: 22956539]

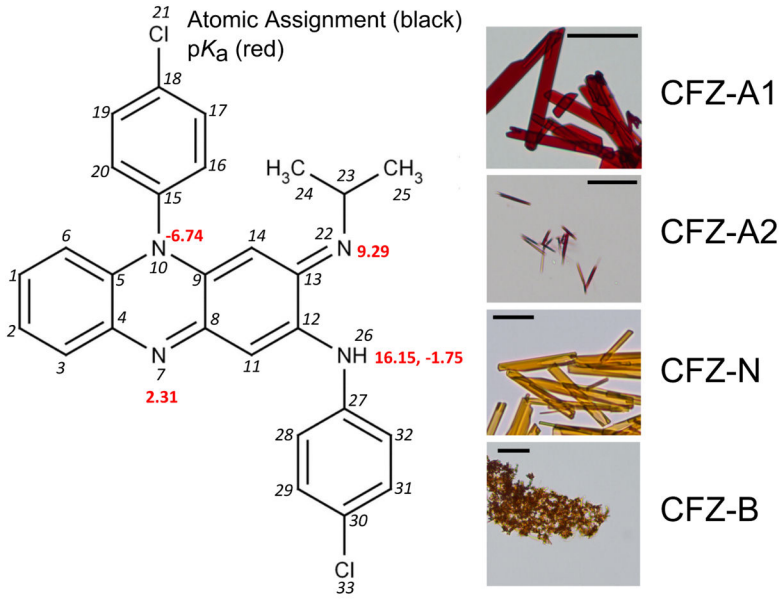


**Figure 1.**

CFZ with atomic assignment for $^{1}$H NMR identification and p$K_a$ values. The atomic assignment is used to assign peaks for NMR in Figures 3a, **S5–S15**. Representative brightfield microscopy of CFZ precipitates formed using 0.1 M HCl (CFZ-A1), 1 M $NH_4Cl$ (CFZ-A2), $H_2O$ (CFZ-N) and 0.1 M NaOH (CFZ-B) are shown on the right. Scale bar = 10 μm.

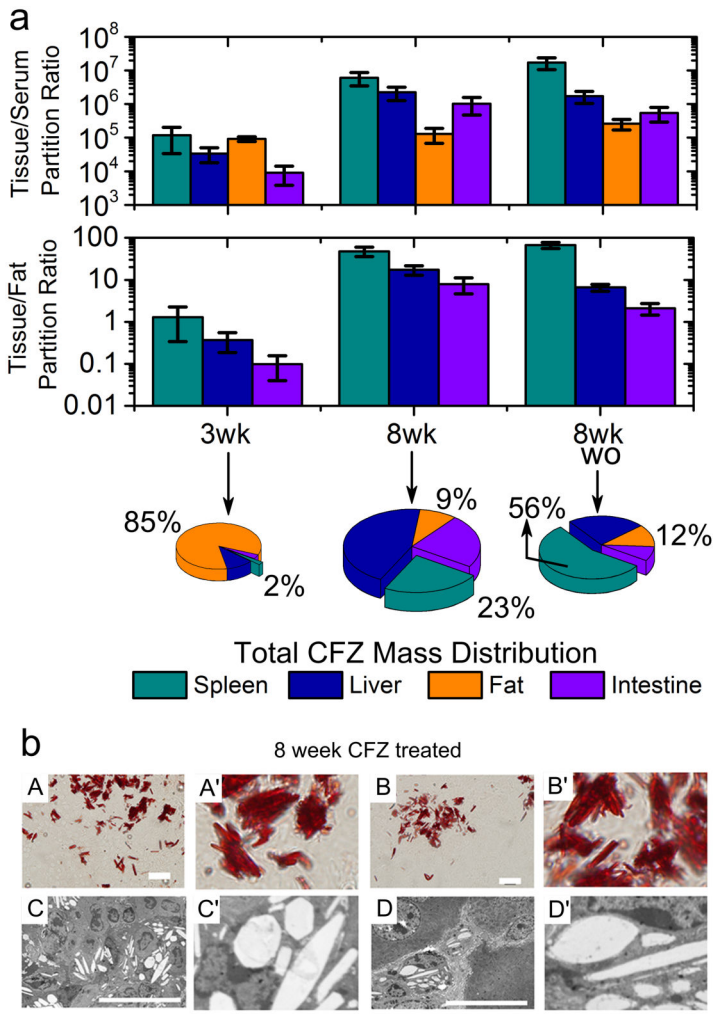


**Figure 2.**

(a) Partition ratios of CFZ in spleen, liver, and intestine, in relation to serum and fat tissue at the major sequestration sites at three weeks (3wk), eight weeks (8wk) and eight weeks + eight weeks washout (8wk wo). All partition coefficients were significantly different between 3wk, 8wk and 8wk wo ($p<10^{-6}$, spleen; $p<10^{-3}$, liver; $p<10^{-2}$, intestine). Pie charts showing fractional mass distribution of clofazimine in the four major drug disposition sites in the mice at 3 wk, 8wk and 8 wk wo. The area of each pie corresponds to the total drug mass. Although total mass decreased during washout, spleen mass (exploded pie) increased significantly (Student's t-test, $p<0.05$). (b) Bright field optical microscopy revealed red clofazimine CLDIs in (A) spleen and (B) liver tissues at 8 weeks (scale bar = 20 μm). (A′–B′) Zooming into relevant regions in A and B. TEM images of fixed (C) spleen and (D) liver cryo-sections revealed the corresponding empty (white) CLDI cavities following extraction of clofazimine during the sample preparation process (scale bar = 20 μm). (C′, D′) Zooming into relevant regions of the images shown in C and D.

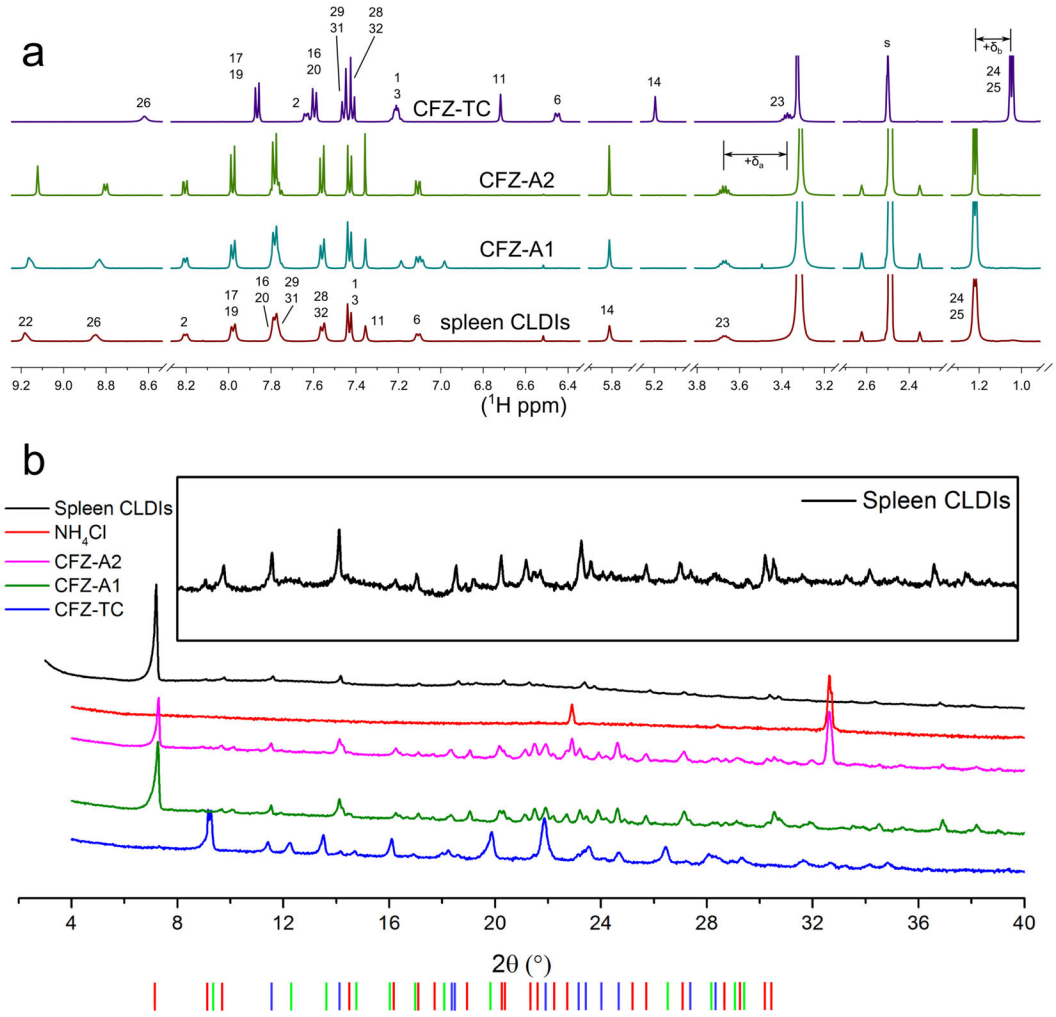


**Figure 3.**

(a) Representative $^{1}$H NMR spectra of spleen CLDIs, CFZ-A1, CFZ-A2 and CFZ-TC, s – residual solvent peak. The amine proton (22) is absent CFZ-TC while all other protons undergo a +δ shift with respect to CFZ-TC in CFZ-A1, CFZ-A2 and CLDIs confirming the monoprotonated characteristic of the molecule in these samples. The NMR spectrum of CLDIs, CFZ-A1 and CFZ-A2 corresponded to identical protonation states of the molecule. (b) Powder X-Ray Diffraction (p-XRD) of spleen CLDIs, CFZ-A1, CFZ-A2 and CFZ-TC showing peaks (crystal diffraction planes) common to CLDIs, CFZ-A1 and CFZ-A2 (red vertical bars), exclusive to CFZ-TC (green vertical bars) and in all samples (blue vertical bars). Inset shows spleen CLDIs p-XRD. The signature peak of CLDIs at 2θ = 7.2° is absent in CFZ-TC while prominent in CFZ-A1 and CFZ-A2. Conversely, the peak at 2θ = 9.3° visible in CFZ-TC is absent in the other CFZ samples.

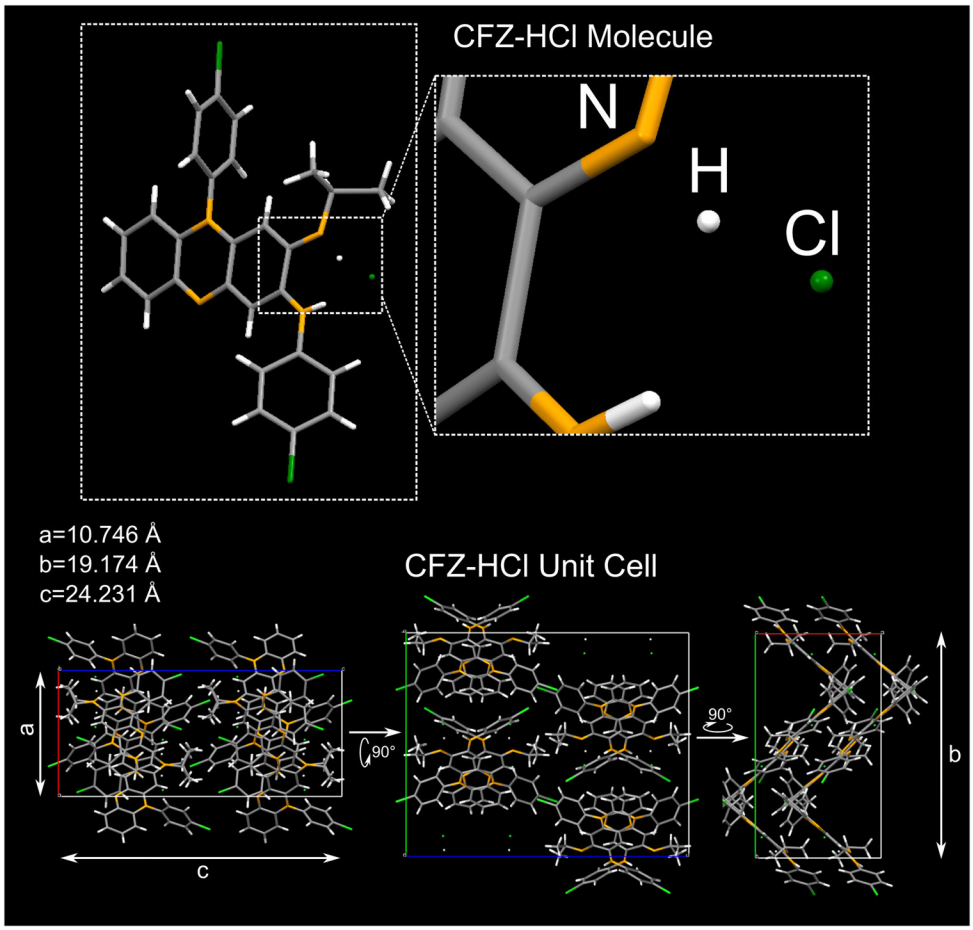


**Figure 4.**

CFZ-HCl crystal structure shown in three orthogonal views to depict the unit cell comprising of 8 CFZ-HCl molecules. Cl is shown in green, N in orange, H in white and C in grey. Unit cell dimensions are a, b and c. All unit cell angles (α, β and γ) are at 90°.

**Table 1**

Bulk Elemental Composition Analysis (BEA) for CFZ-TC, CFZ-A1, CFZ-A2 (on % impurity-free basis).

| Element | CFZ-TC | CFZ-A1 | CFZ-A2 |
|---|---|---|---|
| C | 68.47 | 63.15 | 63.15 |
| H | 4.82 | 4.66 | 4.66 |
| N | 11.82 | 10.91 | 10.91 |
| Cl | 14.89 | 21.28 | 21.28 |
| S | 0.00 | 0.00 | 0.00 |
| Stoichiometry | CFZ | CFZ+H+Cl | CFZ+H+Cl |
| N/Cl (atomic) | 2 | 1.33 | 1.33 |

**Table 2**

Elemental ratios through the depth of sputtering obtained via nanoSIMS. Atomic counts were normalized and calibrated using CFZ-TC as calibration standard. Graphical representation of depth profile is shown in Figure S16. Representative mass images of N, C, P, S, Si, O and Cl are shown in Figure S17.

| | N/Cl | C/Cl | P/Cl | S/Cl | Si/Cl | O/Cl |
|---|---|---|---|---|---|---|
| CFZ-TC | 2.00 | 13.50 | 0.00 | 0.00 | 0.00 | 0.00 |
| CLDIs | 0.21 | 23.16 | 0.00 | 0.00 | 0.00 | 0.02 |
| CFZ-HCl | 1.33 | 4.43 | 0.00 | 0.00 | 0.00 | 0.00 |
| Tissue only | 50.14 | 81.59 | 0.13 | 0.92 | 0.12 | 1.70 |